International Journal of Heat and Mass Transfer 52 (2009) 2528–2542

Contents lists available at ScienceDirect

International Journal of Heat and Mass Transfer

journal homepage: www.elsevier.com/locate/ijhmt

An Eulerian/Lagrangian method for the numerical simulation of incompressible convection flows interacting with complex obstacles: Application to the natural convection in the Lascaux cave

Delphine Lacanette [a,c,*], Stéphane Vincent [a,c], Arthur Sarthou [a,c], Philippe Malaurent [b], Jean-Paul Caltagirone [a,c]

[a] University of Bordeaux, Transferts, Écoulements, Fluides, Énergétique (TREFLE), UMR CNRS 8508 Site ENSCPB, 16 Avenue Pey-Berland, 33607 PESSAC Cedex, France
[b] University of Bordeaux, Géosciences, Hydrosciences, Matériaux, Construction (GHYMAC), Avenue des Facultés, 33405 TALENCE Cedex, France
[c] CNRS, Laboratoire TREFLE, Pessac Cedex, F33607, France

ARTICLE INFO

Article history:
Received 18 March 2008
Received in revised form 8 December 2008
Available online 9 March 2009

Keywords:
Incompressible flows
Natural convection
Penalty methods
Lascaux cave
Fictitious domains
Eulerian/Lagrangian grid coupling

ABSTRACT

An Eulerian/Lagrangian method for the numerical simulation of incompressible convection flows interacting with complex obstacles is developed in this article. This method is successfully validated on natural convection cases, a porous medium and the Sierpinski carpet. The ability of the model to take accurately into account complex topologies allows its application to natural convection in the Lascaux cave, in order to give information on velocities, temperature and moisture content values and to provide helpful details to the conservators of the cave.

1. Introduction

Designing a numerical model to deal with natural convection in cavities as well as the conduction into the rock surrounding the cave is of major importance for the conservation of confined areas. Moreover, the complex topology of the cave has to be accurately taken into account by the numerical tool. Two approaches are currently encountered. On the one hand, using body-fitted unstructured grid [1,2] the method consists in considering two subdomains with their own grids. They are connected by a boundary condition corresponding to the interface between the solid and the fluid media. The solutions in each subdomain are connected thanks to jump conditions on mass, momentum and energy. The main advantages of unstructured methods are that they naturally take into account the complex shape of the objects and they provide an explicit description of the interface between the media, in order to apply the real physical jump or transmission conditions. Concerning the drawbacks of this method, the grid generation is complex and even impossible due to the strong irregularities of the fluid–solid interface. On the other hand, another numerical methodology for treating the fluid–solid interaction is the fictitious domain approach developed during the last 15 years by many authors [3–6] or [7]. This technique is based on the concept of using a structured grid for dealing with conservation equations such as the Navier–Stokes or energy equations. The obstacles or solids are drawn into the structured simulation grid and specific terms are added to the conservation equations in order to account for the presence of obstacles. The major advantages of this method are its readiness to implement, even in three dimensions and its ability to be integrated to existing CFD tools. Furthermore, it can deal with moving solids and several approaches have been extended to high order [7] or [8]. The main drawback is the relative lack of accuracy in the description of the boundary layers as the grid is not *a priori* adapted to the shape of the obstacles.

The management of complex shaped objects, such as those involved in the last section of this paper, requires months of work with grid generators in order to build unstructured meshes of good quality in the fluid and solid media. In addition, if moving solid objects interact with the flow motion, the 3D unstructured grid must be updated by means of an automatic procedure. This operation is not possible in certain situations. For all these reasons, we have chosen to simulate the natural convection in a complex shape cave using the fictitious domain approach and penalty methods, following the works [3,4,9,8].

The Lascaux cave, discovered in 1940 and located in the Dordogne area in France, is inscribed on the Unesco World Heritage List. It is considered as one world's major prehistoric caves. Since its

* Corresponding author. Address: CNRS, Laboratoire TREFLE, Pessac Cedex, F33607, France. Tel.: +33 5 40 00 28 31; fax: +33 5 40 00 66 68.
E-mail address: lacanette@enscpb.fr (D. Lacanette).

0017-9310/$ - see front matter © 2009 Elsevier Ltd. All rights reserved.
doi:10.1016/j.ijheatmasstransfer.2008.12.028

Nomenclature

Latin letters

a	thermal diffusivity (m^2/s)
C_P	specific heat (J/kg K)
dr	augmented Lagrangian parameter (Pa.s)
D	diffusion coefficient (m^2/s)
D_h	hydraulic diameter (m)
E	characteristic dimension (m)
F_C	moisture source term (g/kg dry air s)
$\mathbf{g}$	gravity vector (m/s^2)
h	exchange coefficient (W/m^2 K)
K	permeability (m^2)
p	pressure (Pa)
T	temperature (K)
t	time (s)
$\mathbf{u}$	velocity (m/s)

Greek symbols

β	expansion coefficient (K)
λ	conductivity (W/m K)
μ	dynamic viscosity (Pa s)
ϕ	absolute moisture content (g/kg dry air)
ρ	density (kg/m^3)
χ	color function

Subscripts and superscripts

f	fluid medium
s	solid medium
I	interface

Non-dimensional

$Ra = \frac{\rho^2 C_P g \beta \Delta T E^3}{\mu\lambda}$ Rayleigh number

$Da = \frac{hE}{\lambda}$ Darcy number

$Le = \frac{a}{D}$ with $a = \frac{\lambda}{\rho C_P}$ Lewis number

$Nu = \frac{hE}{\lambda}$ Nusselt number

$Pr = \frac{\mu C_P}{\lambda}$ Prandtl number

$Ra^* = Ra\ Da = \frac{\rho^2 C_P g \beta \Delta T E^3}{\mu\lambda}\frac{K}{E^2}$ filtration Rayleigh number

$Sc = \frac{\mu}{\rho D}$ Schmidt number

discovery, several problems have occurred, due to the huge amount of visitors [10], and their release of vapor and carbon dioxide by their breath, causing the formation of calcite and the apparition of green algae and mosses. The Minister of Cultural Affairs (André Malraux) had the cave closed in 1963.

The closure solved some of the problems for a while and the Lascaux cave art returned to the state it was in the day of the discovery. Since then, prehistorians, archeologists, geologists, hydrogeologists, have tried hard to maintain the cavity in the most stable state possible, using remote metering to record the variations in temperature, hygrometry, and carbon dioxide gas pressure. The biological equilibrium remained fragile and in 2001 colonies of micro-organisms, fungi and bacteria developed on the rock edges and on the floor. This attack made the authorities and the Minister of Culture and Communication create an international committee of the Lascaux cave. This multidisciplinary committee is composed of archeologists, physicists, geologists, hydrogeologists and conservators working altogether to understand the mechanisms of apparition of the micro-organisms in order to stop their propagation. Since then, biologists have developed treatments and complex processes to eradicate these micro-organisms [11,12].

In the process of time the temperatures and hydric conditions have often changed [13]. Under the influence of exchanges and energy transfers with the outside, the system formed by the Lascaux cave evolved and its state variables have been modified. Climate change had consequences which occurred before its discovery which can be observed in the paintings on various places of the cave.

Among the measures taken by the committee, a better understanding of the flows in the cave was deemed a paramount importance, and has induced the creation of a simulation tool, the "Lascaux Simulator". The nonintrusive character of the simulation is one of the major assets of this method. Thus, the numerical simulation in fluid mechanics is here dedicated to the conservation of the Lascaux cave. It has previously been studied by Ferchal [14,15] with the CFD code developed by EDF on an unstructured grid. The present work constitutes a different view of the problem, using a fictitious domain approach [16,17].

The numerical methodology used in this paper is first exposed. The governing equations and the numerical modeling of solid walls are detailed. Then the method is validated on two different cases, the natural convection in a porous medium, and the case of Sirpinski carpet. Finally, the method is applied to the study of the natural convection in the Lascaux cave, and information about the distribution of temperature and moisture contents considering different thermal configurations is provided.

2. Numerical methodology

2.1. Conservation equations

In the fluid medium (see Fig. 1) Ω_f, the conservation equations describing the unsteady incompressible convection flows of a

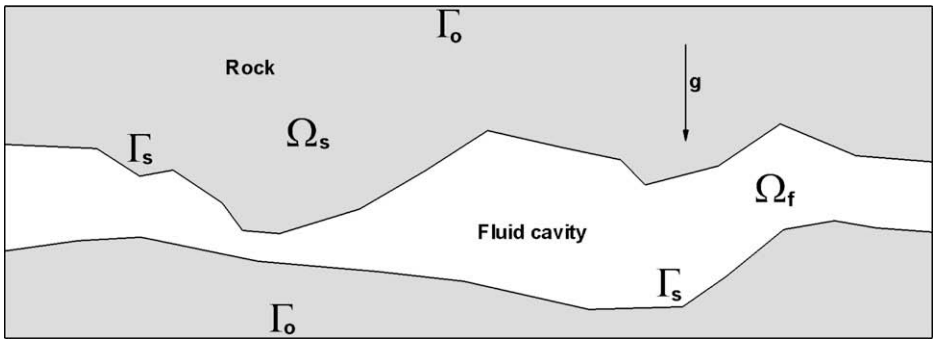

Fig. 1. Definition sketch.

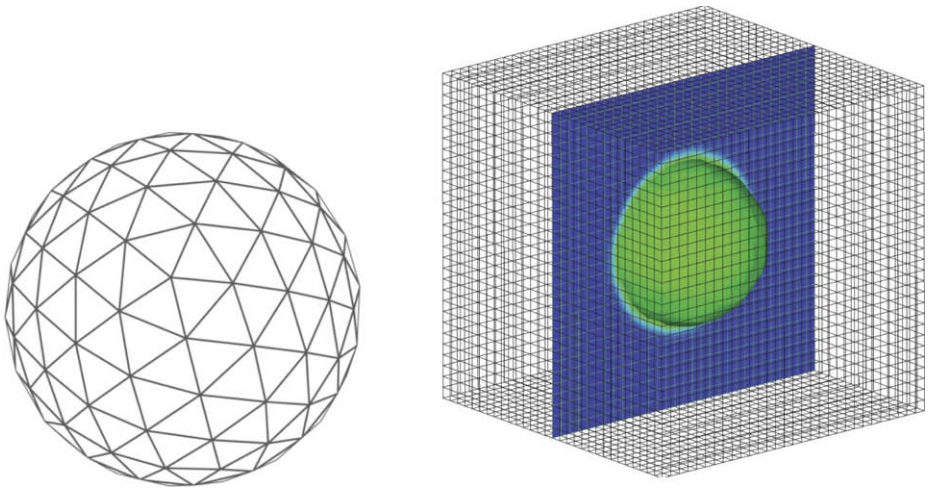

Fig. 2. Example of Lagrangian grid and corresponding projected solid fraction χ (the $\chi = 0.5$ isosurface and isocontours of χ in a slice are plotted).

Newtonian fluid and the evolution of the moisture concentration, under the Boussinesq approximation, are the Navier–Stokes, energy and transport of moisture concentration equations written in terms of velocity and temperature:

$$\rho\left(\frac{\partial \mathbf{u}}{\partial t} + \nabla\cdot(\mathbf{u}\otimes\mathbf{u})\right) = -\nabla p + \rho\mathbf{g} + \nabla\cdot(\mu[\nabla\mathbf{u} + \nabla^T\mathbf{u}]) \tag{1}$$

$$\nabla\cdot\mathbf{u} = 0 \tag{2}$$

$$\rho C_P\left(\frac{\partial T}{\partial t} + \mathbf{u}\cdot\nabla T\right) = \nabla\cdot\lambda\nabla T \tag{3}$$

$$\left(\frac{\partial \phi}{\partial t} + \mathbf{u}\cdot\nabla\phi\right) = \nabla\cdot(D\nabla\phi) \tag{4}$$

It is assumed that λ, C_P, D and μ are constant with respect to T. The density variations are described by the following linear expression:

$$\rho(T) = \rho_0(1 - \beta[T - T_0]) \tag{5}$$

In the solid part Ω_s, the velocity is assumed to be negligible. Only conduction effects drive the thermal exchanges in this case. We have

$$\mathbf{u} = 0 \quad \text{and} \quad \phi = 0 \tag{6}$$

$$\rho C_P\frac{\partial T}{\partial t} = \nabla\cdot\lambda\nabla T \tag{7}$$

The boundary conditions for the velocity, temperature fields and moisture content concentration are the following:

$$\mathbf{u} = 0 \quad \text{and} \quad -\lambda_f\frac{\partial T_f}{\partial n} = -\lambda_s\frac{\partial T_s}{\partial n} \quad \text{and} \quad \phi = 0.5545\times T + 1.8909 \text{ on } \Gamma_s \tag{8}$$

$$\mathbf{u} = 0 \quad \text{and} \quad \frac{\partial T_s}{\partial n} = 0 \quad \text{and} \quad \phi = 0 \text{ on } \Gamma_o \tag{9}$$

2.2. Numerical modeling of solid walls

2.2.1. Management of the fluid/solid interface

The present work aims at proposing a numerical method which is able to deal with fluid/solid interaction while using structured grids non conforming to the complex shape of the obstacles. The main idea is a continuation of the previous works of Caltagirone et al. [18,3] concerning fictitious domains. The method is structured as follows:

⊗ the simulation domain $\Omega = \Omega_s \cup \Omega_f$ which includes both the fluid and solid zones is discretized with a global structured grid *a priori* not adapted to Γ_s. On this Eulerian grid, standard numerical methods apply (see below).

⊗ the topology of the fluid/solid interfaces is not explicitly known on the Eulerian structured grid which doest not fit to Γ_s. As a consequence, the jump conditions cannot be explicitly implemented in Eqs. (5)–(9). The fictitious domain approach consists in introducing local volume effects in the conservation equations so as to account for the volume effect of the solid medium in Ω_s. In a first step, a triangular Lagrangian grid $\mathbf{x}_f$ of the solid zones is projected onto the Eulerian grid (see Fig. 2) by solving a diffusion equations as follows [19]:

$$\Delta\chi = \nabla\cdot\int_{\Gamma_s}\mathbf{n}_i(\mathbf{x} - \mathbf{x}_f)\delta_i ds \tag{10}$$

where χ is the local volume fraction of the solid, $\mathbf{n}_i$ is the normal to Γ_s, $\mathbf{x}$ is a location on the Eulerian grid and δ_i is the Dirac function indicating the interface. After solving Eq. (10), $\chi = 1$ in Ω_s and 0 elsewhere. The interface Γ_s between Ω_f and Ω_s is defined as $\chi = 0.5$.

⊗ function χ allows us to locate the solid and fluid part on the Eulerian grid. A Darcy term is added to the momentum equations in order to penalize the solid behavior through the conservation equations. The new penalty Navier–Stokes Brinkman model so obtained, which replaces Eq. (1), reads:

$$\rho\left(\frac{\partial \mathbf{u}}{\partial t} + \nabla\cdot(\mathbf{u}\otimes\mathbf{u})\right) + \frac{\mu}{K}\mathbf{u} = -\nabla p + \rho\mathbf{g} + \nabla\cdot(\mu[\nabla\mathbf{u} + \nabla^T\mathbf{u}]) \tag{11}$$

where $K = +\infty$ if $\chi < 0.5$ and $K = 0$ if $\chi \geqslant 0.5$. To sum up, our fictitious domain method uses penalty terms added to the momentum conservation equations to model the presence of solid obstacles.

2.2.2. Management of humidity transfer

The humidity transfer is estimated directly on the real Lagrangian surface rather than the projected Eulerian one. It is made of two steps.

1. The temperature gradient in the normal direction for each surface triangle $\mathbf{S}_l$ is first calculated as follows:
   - ⊗ a normal vector $\mathbf{N}_l$ to $\mathbf{S}_l$ is defined. It is oriented toward the fluid medium, starting from the barycenter of $\mathbf{S}_l$ and its length is the local grid space.
   - ⊗ the temperatures T_b and T_f, respectively, at the barycenter and in the fluid, i.e. at the edges of $\mathbf{N}_l$, are evaluated by linearly interpolating the Eulerian field.
   - ⊗ the temperature gradient is directly obtained by $\nabla_\perp T_l = \frac{T_f - T_b}{\|\mathbf{N}_l\|}$.

2. A specific penalty term is added in Eq. (4) in order to impose the moisture content in the cell cut by the air/rock interface:

$$\frac{\phi^{n+1}-\phi^{n}}{\Delta t}+\mathbf{u}^{\mathbf{n+1}}\cdot\nabla\phi^{n+1}=\nabla\cdot(D\nabla\phi^{n+1})+B\left(\phi^{n+1}-f(\nabla_{\perp}T_{I}^{n})\right) \tag{12}$$

where B is a penalty coefficient equal to 10^{40} in the cells cut by the interface and 0 elsewhere, and f is a function based on an energetic balance between the heat driven by the conduction through each triangle and the energy necessary to evaporate or condensate all the vapor contained in an elementary volume of the Eulerian grid. The normal temperature gradient to the interface is $\nabla_{\perp}T_{I}$. It is calculated on the Lagrangian interface and is projected on the Eulerian grid to build f.

2.3. Discretization and solvers

The system of Eqs. (1)–(9) which describes the interaction between the natural convection in a cavity and the conduction in the rock is discretized thanks to implicit finite volumes [20] on a fixed staggered Cartesian Marker And Cell (MAC [21]) grid. In Ω_f, the coupling between pressure and velocity, as well as the incompressibility constraint, are fulfilled by using a minimization algorithm called augmented Lagrangian [22]. The time derivatives are discretized by first order Euler schemes, whereas the spatial derivatives are approximated by centered schemes.

The implicit discretization of the momentum and energy equations involves the solving of a linear system $A^{n}X^{n+1}=F^{n}$ by using an iterative BiCGSTAB solver [23], preconditioned under a Modified and Incomplete LU (MILU) method [24]. The index n is related to time $n\Delta t$ for which Δt is the time step. The mass and momentum equations are first solved by the augmented Lagrangian method in order to obtain $(\mathbf{u}^{n+1},p^{n+1})$ as follows:

$$\begin{aligned}
&k=0, p^{0}=p^{n} \quad \text{and} \quad \mathbf{u}^{0}=\mathbf{u}^{n}\\
&\text{Solve}\\
&k=k+1\\
&\rho^{n}\left(\frac{\mathbf{u}^{k}-\mathbf{u}^{n}}{\Delta t}+\nabla\cdot(\mathbf{u}^{k-1}\otimes\mathbf{u}^{k})\right)\\
&\quad=-\nabla p^{k-1}+dr\nabla(\nabla\cdot\mathbf{u}^{k})\\
&-\frac{\mu}{K}\mathbf{u}^{k}+\rho\mathbf{g}+\nabla\cdot(\mu[\nabla\mathbf{u}^{k}+\nabla^{T}\mathbf{u}^{k}])\\
&p^{k}=p^{k-1}-dr\nabla\cdot\mathbf{u}^{k}\\
&\text{While}\nabla\cdot\mathbf{u}^{k}\geqslant\epsilon|
\end{aligned} \tag{13}$$

where ϵ is chosen equal to almost zero computer error ($\epsilon=10^{-15}$ in double precision calculations). At the end of the minimization procedure, we assume that $\mathbf{u}^{n+1}=\mathbf{u}^{k}$ and $p^{n+1}=p^{k}$. The minimization parameter dr can be set constant or determined automatically by analyzing the physical or numerical parameters of the problem [25,26]. In our simulations, the augmented Lagrangian parameter $dr=1$ as the local variations of density and viscosity are small. In addition, the permeability is chosen equal to 10^{40} in the fluid and 10^{-40} in the solid. The magnitude of K has no effect on the efficiency of the iterative solver as the permeability only affects diagonal coefficients in the linear system. More details on the convergence order and behavior of the penalty method are given for example in [3].

Then, the temperature T^{n+1} is obtained by:

$$\rho^{n}C_{P}\left(\frac{T^{n+1}-T^{n}}{\Delta t}+\mathbf{u}^{n+1}\cdot\nabla T^{n+1}\right)=\nabla\cdot\lambda\nabla T^{n+1}$$

To finish with, the vapor concentration ϕ^{n+1} is obtained by:

$$\phi^{*}=\phi^{n}+\Delta t*B(\phi^{*}-f(\nabla_{\perp}T_{I}^{n}))$$

$$\left(\frac{\phi^{n+1}-\phi^{*}}{\Delta t}+\mathbf{u}^{n+1}\cdot\nabla\phi^{n+1}\right)=\nabla\cdot D\nabla\phi^{n+1}$$

More information, details and validations about the discretizations and solvers have been extensively investigated in previous works [3,27].

3. Validation

3.1. Natural convection in a porous medium

Following the works of Arquis [28], the interest and accuracy of the Brinkman penalty method can be illustrated by simulating on a local scale the natural convection in a square cavity, differentially heated between a cold temperature wall T_c and a hot one T_h, in which cylindrical inclusions are placed following a square shaped periodical network (see Fig. 3). It is assumed that the conductivity of the cylindrical obstacle is the same as the fluid. Under the action of gravity, natural convection flows develop in the cavity between the cylinders. The main dimensionless parameter of the problem is the Rayleigh number Ra. The Prandtl number of the problem is assumed to be equal to 1.

It is proposed to consider several configurations in which the porosity is constant and equal to 0.615 and the number of cylinders N is increased progressively from 4^2 to 32^2. Due to the presence of the obstacles, the flow velocities are decreased and the cavity behaves as a porous medium. In order to take into account the effects of the cylinders on the convection, a modified Rayleigh number, called the filtration Rayleigh number, is introduced. Ra^{*} is equal to the product between the classical Rayleigh and the Darcy number. In the following simulations, Ra^{*} is assumed constant and equal to 122.6.

We consider three convection cases where N of 4^2, 8^2 and 32^2, are associated to 64^2, 256^2 and 512^2 simulation grids, respectively. The stationary results of temperatures, streamlines and obstacles are presented in Fig. 5. For $N=4^2$, the isotherms are irregular, demonstrating a different thermal behavior in fluid and solid media. In this case, a macroscopic analysis of the results is not possible. On the contrary, for higher values of N, the flow and temperature isolines are smoother. A macroscopic study is suitable in these configurations.

A quantitative exploitation of the simulations is interesting by analyzing the evolution of the global thermal exchanges in the cavity in terms of Nusselt number Nu. The values of Nu according to $1/N$ are presented in Fig. 4. They all have been obtained with the penalty Brinkman method, except for $1/N=0$ where a Darcy model has been used to simulate this case in particular, assuming a full porous cavity. As a reference, the limit value of the Nusselt number is obtained by simulating with our model a porous medium throughout the whole cavity. This case can be compared to a cavity containing an infinity of cylinder, such as $N\rightarrow+\infty$. It can be observed that when N takes large values, the asymptotic value of the Nusselt number tends to the reference value of $Nu=3.574$ obtained with the Darcy penalty model ($Ra\,Da=122.6$).

To sum up, it has been demonstrated that the Darcy penalty method is able to provide a local description of the interaction between natural convection flows and obstacles in a closed cavity. In terms of thermal exchange, the numerical model is accurate and the reference value of 3.574 of a porous medium is recovered in terms of Nusselt number. This test case validates the choice of the Darcy penalty method for simulating the convection flows in the Lascaux cave which highly depend on the fluid–solid interactions.

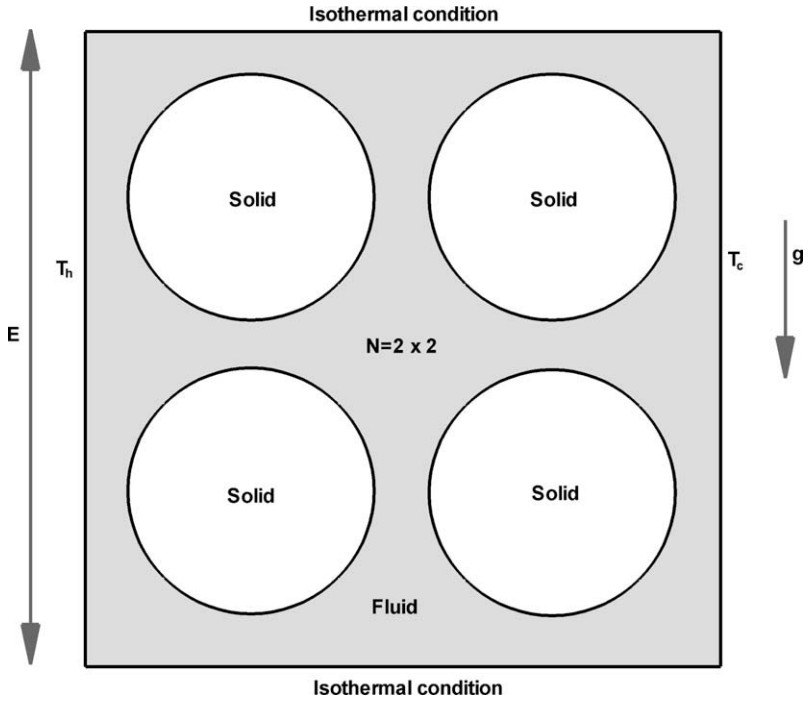

Fig. 3. Definition sketch of the natural convection in a cavity.

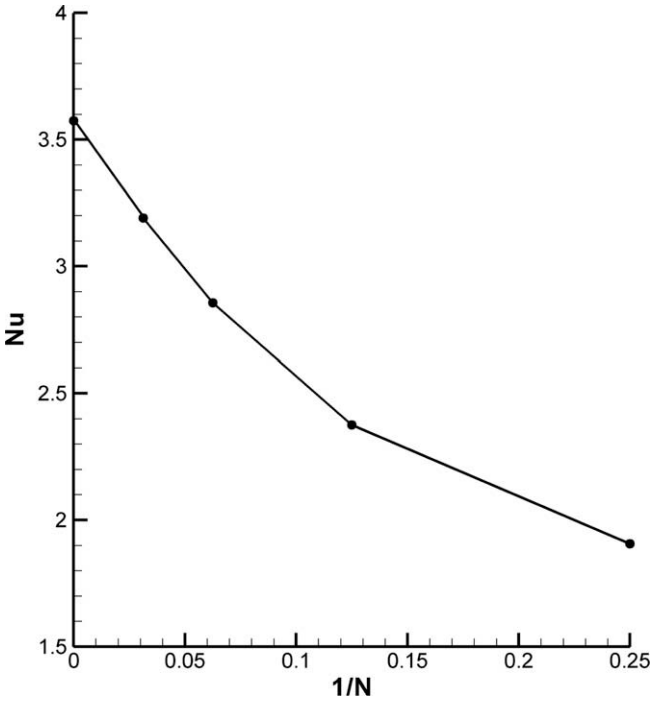

Fig. 4. Evolution of the Nusselt number according to the number N of obstacles in the cavity.

3.2. The Sierpinski carpet

Our purpose in this section is to validate the methodology used to simulate the thermal convection in a 3D cavity comparing simulations with experimental measurements. In [29], Amine et al. compare their numerical results for the Sierpinski carpet case obtained with both experiments and simulations. As the case is not exactly the same for the two methods, experimental and numerical results agree concerning the shape, temperature and velocity profiles. However, the magnitude of the maxima varies in the 20–30% range. Our aim here is to compare the results in [29] with our results in order to demonstrate the validity of our penalty approach.

The Sierpinski carpet is a fractal model composed of squares of various sizes. Fig. 6 illustrates the first three generations of the model. The empty cell is a $100 \times 100\ \text{mm}^2$ box. We impose adiabatic conditions on the upper and lower walls, and a Dirichlet condition of 20 °C and 25 °C on the left and right walls. For all simulations, the liquid used has the following properties: $\mu = 0.0815\ \text{kg/(m s)}$, $\rho = 857\ \text{kg/m}^3$, $C_P = 1880\ \text{J/(kg K)}$ and $\lambda_f = 0.132\ \text{W/(m K)}$. Hence, the Prandtl number Pr is equal to 1160. Obstacles are in plexiglas for which the thermal conductivity is $\lambda_s = 0.19\ \text{W/(m K)}$.

3.2.1. First generation

The obstacle is located between $33.3\ \text{mm} \leqslant x \leqslant 66.7\ \text{mm}$ and $33.3\ \text{mm} \leqslant y \leqslant 66.7\ \text{mm}$. 2D and 3D simulations are first performed. Fig. 7 shows the vertical velocity profile $V_z(x)$ from experiments [29] and our 2D (100^2 mesh) and 3D (70^3 mesh with $z = 50\ \text{mm}$) computations. Results for 2D configuration are very similar to the numerical simulations of Amine et al. (not represented) which are relatively far from experiments. In this paper, the authors have some suppositions about the differences between experimental and numerical results. First, contrary to their initial assumption, the lower and upper walls are not really adiabatic. Amine et al. have tried to change the upper and lower boundary conditions to the Stefan condition. The gain for V_x was counterbalanced by a loss of quality for V_z. Another difference between experiments and simulations lies in the real size of the obstacles used in experiments. Commercially available bars used for the experiment had dimensions changing by steps of 1 mm.

The box used for the experiment has a depth of only 85 mm. In our opinion the flow can have some 3D structures that cannot be represented by 2D simulations due to confinement effects. As can

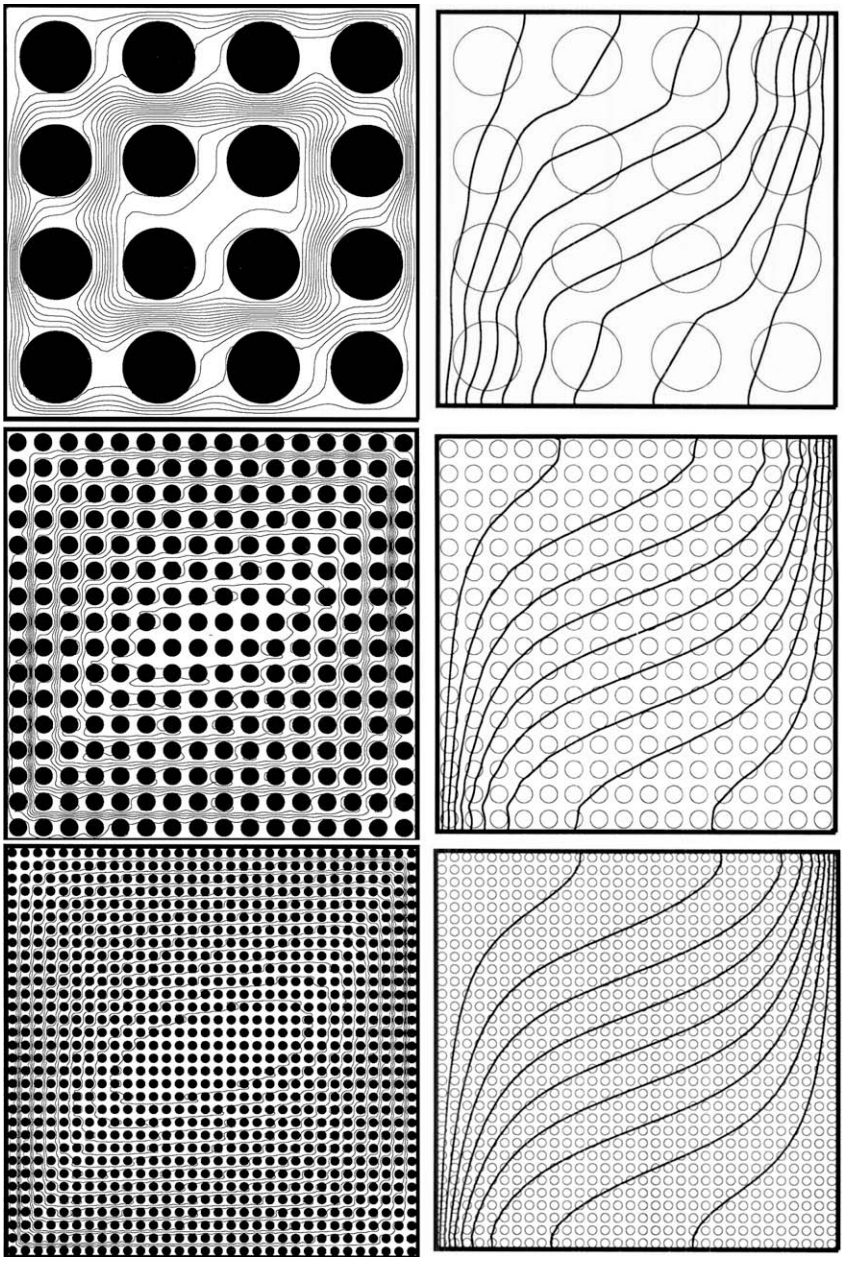

Fig. 5. 2D simulation of the natural convection in a cavity filled with various amounts N of cylinders-$N = 4 \times 4$ with a 64^2 grid, $N = 16 \times 16$ with a 256^2 grid, $N = 32 \times 32$ with a 512^2 grid-left column: streamlines, right column: temperature profiles.

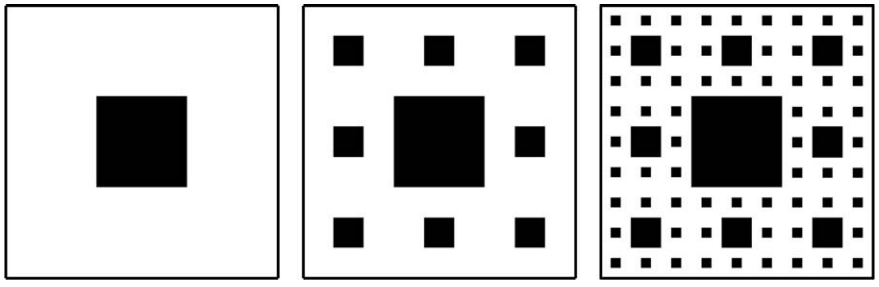

Fig. 6. Sierpinski carpet of 1st, 2nd and 3rd generation.

be seen on Fig. 7, the results obtained with our 3D simulation are closer to the experiment. The difference between the 2D and 3D flow is then studied. Fig. 7 shows the evolution of V_x, V_y and T along the y axis for $z = 10$ mm and $x = 50$ mm. The velocity V_x

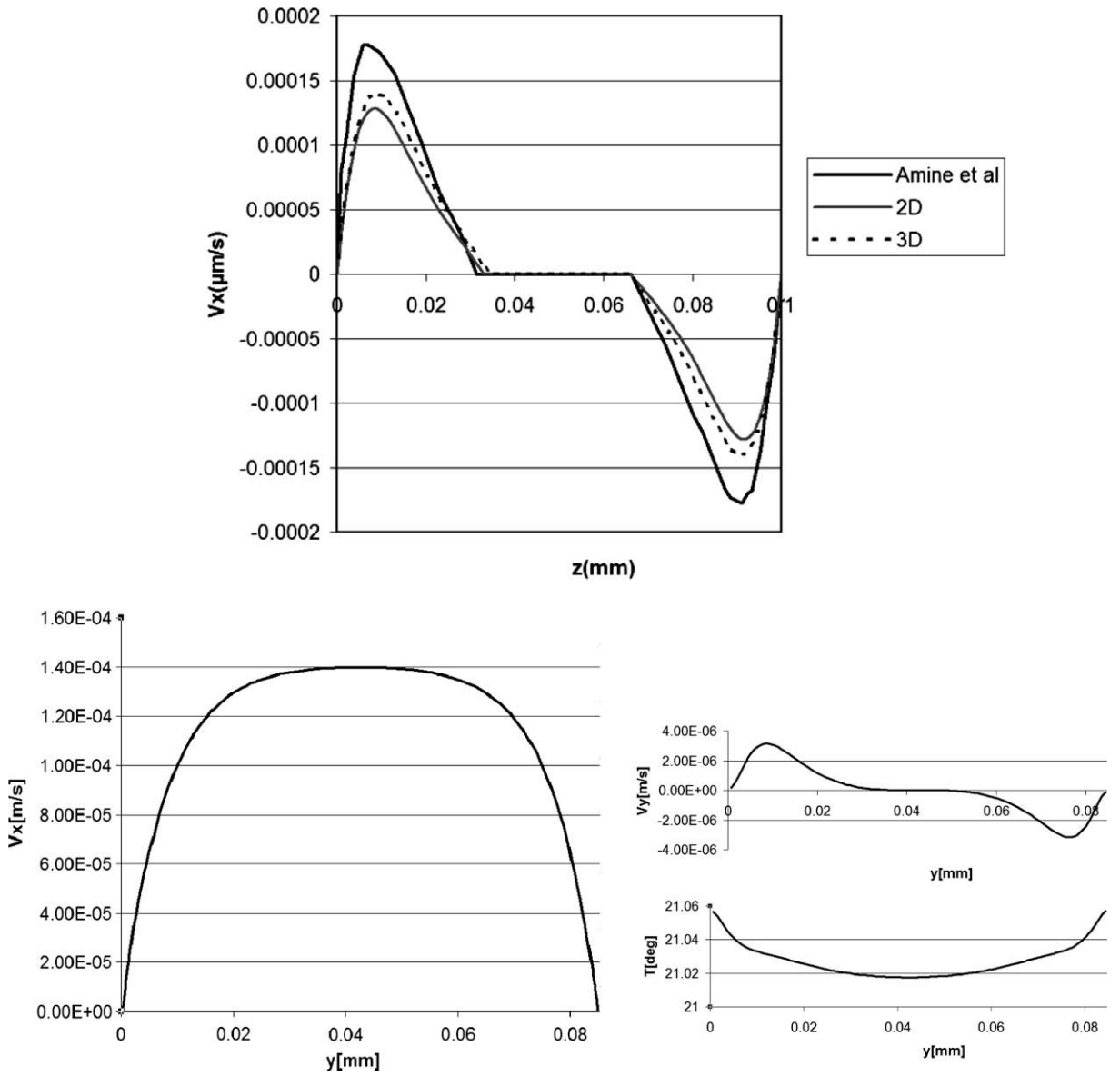

Fig. 7. 3D simulation for the Sierpinski carpet of 1st generation. Horizontal velocity profile $V_x(z)$ at $x = 50$ mm for experiments and numerical simulations (top), values $V_x(y),\ V_y(y),\ T(y)$ for $z = 10$ mm and $x = 50$ mm (bottom).

and the temperature T along the y axis for $y \approx 42.5$ mm are quite stable. This is observed in Fig. 9. The transverse velocity V_y is about two magnitudes smaller than V_x. Hence, the flow is mainly 2D but the effect of the 3D structures is not negligible.

3.2.2. Second generation

A new set of eight additional blocks is considered. The new obstacles are quite small, but the mesh is not chosen to match perfectly with obstacles. The purpose here is to demonstrate the interest of our penalty method even if obstacles do not match the grid. Fig. 8 compares the vertical velocity profile $V_z(x)$ at $z = 17$ mm obtained with experiment and simulation. The 2D (with a 150^2 mesh) and 3D (with a 70^3 mesh) simulations are close to the results obtained by experiment. However, the 3D calculation provides a better agreement.

Fig. 8 shows the velocity profile $V_x(z)$ at $x = 50$ mm. As for the first generation carpet, the correspondence between experiment and simulations is not very good for 2D, even if the results obtained with the 3D simulation on a relatively coarse grid are closer to experiment. The results with an additional 2D simulation with a 300^2 mesh are slightly improved.

Streamlines and sensors position is shown in Fig. 9. As in [29], we observe a negative velocity V_z between the 2nd and 3rd lower obstacles.

3.2.3. Conclusion for the Sierpinski carpet

The experiments of Amine et al. [29] and our numerical simulations have been compared. Even on coarse grids, the main structures of the experimental flows have been well reproduced by our methodology and it has been demonstrated that the 3D character of the flow improves the accuracy of the simulations, compared to the 2D computations of Amine et al. However, for various reasons, for instance the inaccurate modeling of the real boundary conditions, differences on velocities have been observed.

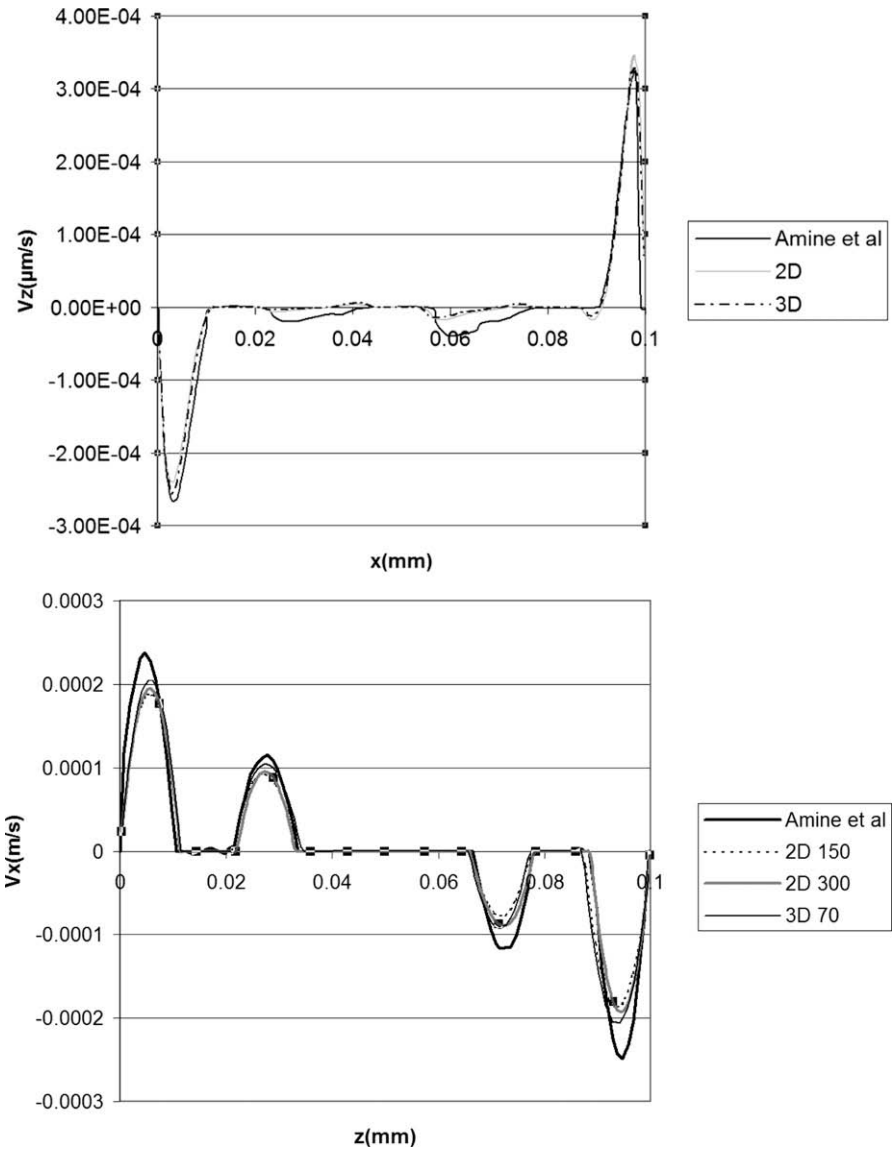

Fig. 8. Sierpinski carpet of 2nd generation. Horizontal velocity profile $V_z(x)$ at $z = 17$ mm (left), horizontal velocity profile $V_x(z)$ at $x = 50$ mm (right) for experiments and numerical simulations.

4. Application to the Lascaux cave

The numerical methodology is applied here to the study of the natural convection in the Lascaux cave. The accurate description of the cavity allows a fine analysis of the flow as well as the moisture content distribution in the cave.

4.1. Initial conditions

The reversal time has been evaluated to 1 h, thus the total simulation time has been fixed to 7 h. The boundary conditions are steady, considering the temperature in the cave is stable during 7 h. Nevertheless, the flow is unsteady, due to the complex geometry and the thermal gradients, as it can be checked in Fig. 10.

4.1.1. Geometry

A three-dimensional survey of the Lascaux cave was made by the land surveyor Perazio using laser scanning. Triangular surface elements of each object interacting with the flow motion are generated. A detail of this surface is shown in Fig. 11. In the following, the gravity acceleration is directed towards the *Y*-axis.

The Lagrangian description of the solid objects is projected onto the fixed Eulerian flow grid as detailed in Section 2.2. The Eulerian view of the geometry as well as reference marks of the Lascaux cave are given in Fig. 11. The global domain of computation is composed of 3.5 million points.

4.1.2. Thermal conditions

Concerning the Rayleigh number, simulations on a differentially heated square cavity are achieved in order to get the evolution of the Nusselt number with the Rayleigh number and to compare the values of velocities with the theoretical ones.

The order of magnitude of the velocity in the boundary layer for high Rayleigh numbers is given by $V_0 = \sqrt{g\beta\Delta T D_h}$. The Table 1 shows a comparison between simulated values of velocity and theoretical ones for a given Rayleigh number.

This comparison is valid for a Rayleigh higher or equal to 10^5, at this point the boundary layers are separated. The order of magnitude of the velocities is the same, the CFD code used as a basis for the simulation in the Lascaux cave gives classical results of natural convection.

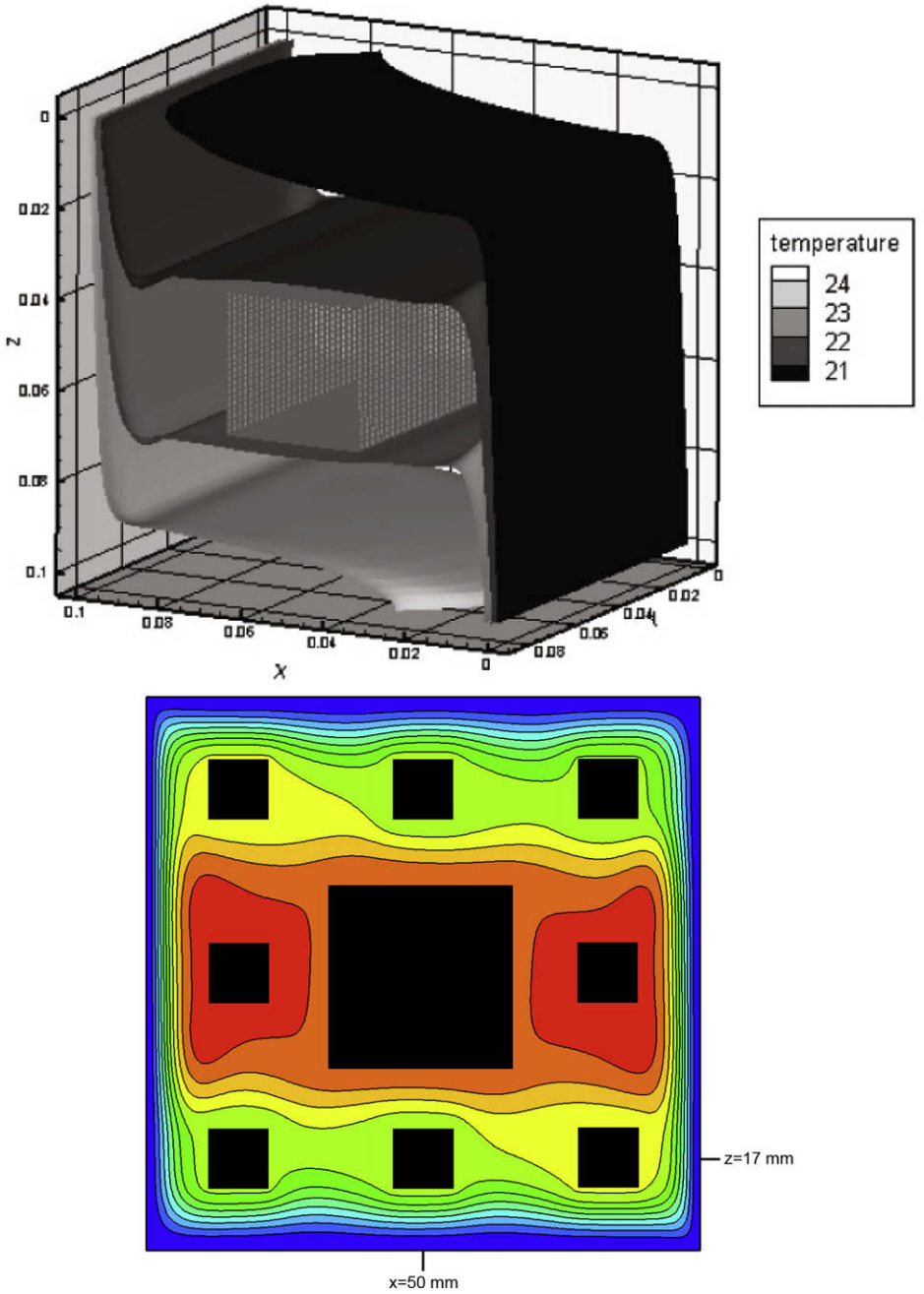

Fig. 9. Isosurfaces of temperature for 3D simulations (top), streamlines for the Sierpinski carpet of 2nd generation (bottom).

The Nusselt numbers corresponding to the simulated velocities have been calculated on a 256×256 Chebyshev grid and compared to reference spectral solutions [30] in Table 2. The calculated values are in good agreement with the benchmark results. Plotting its evolution with the Rayleigh number, the relation (14) is found for a differentially heated square cavity.

$$Nu = 0.17Ra^{0.2821} \tag{14}$$

For a vertical plate, the evolution of the Nusselt number follows the relation (15) [31]:

$$Nu = 0.59Ra^{0.25} \tag{15}$$

This expression is slightly different from the relation (14) due to the containment of the geometry, the boundary layer is finite in the cavity whereas it is considered as infinite in the vertical plate case. Nevertheless the expression (14) is characteristic of a separated boundary layer flow.

In the Lascaux cave, in the thermal configuration of 1981, and without human disturbances, the measured velocities are approximately 5×10^{-2} m/s. Referring to the previous relation, an equivalent Rayleigh number of 10^8 can be given, which corresponds to a differentially heated cavity. This number indicates a laminar flow regime.

The Lewis, Prandtl and Schmidt numbers are, respectively, equal to 1.015, 0.71 and 0.721. The heat, mass and momentum diffusion are of the same order. Thus, the characteristic time and space scales of the involved physical phenomena are compatible; the same time steps and the same grid can be used for all the equations. Our unsteady and deterministic modeling strategy is confirmed by the previous remarks.

The initial conditions in temperature are calculated on a one-dimensional heat conduction model in the floor, based on the temperature measured by Météo France [32] during more than 50

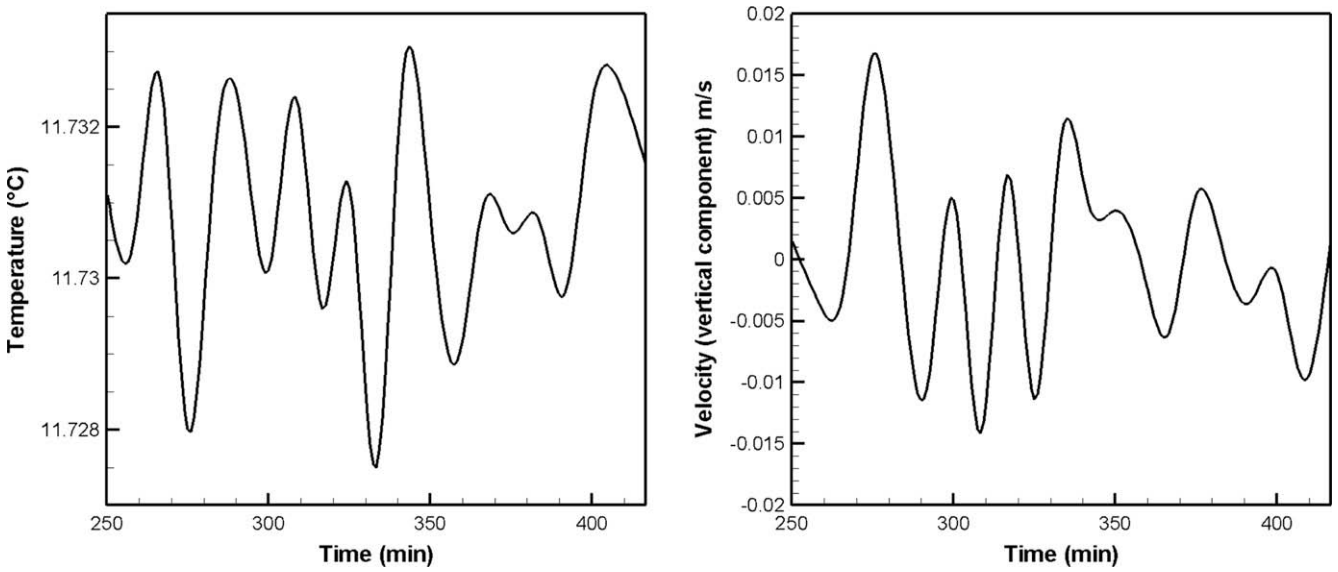

Fig. 10. Evolution of temperature (left) and vertical component of the velocity (right) as a function of time.

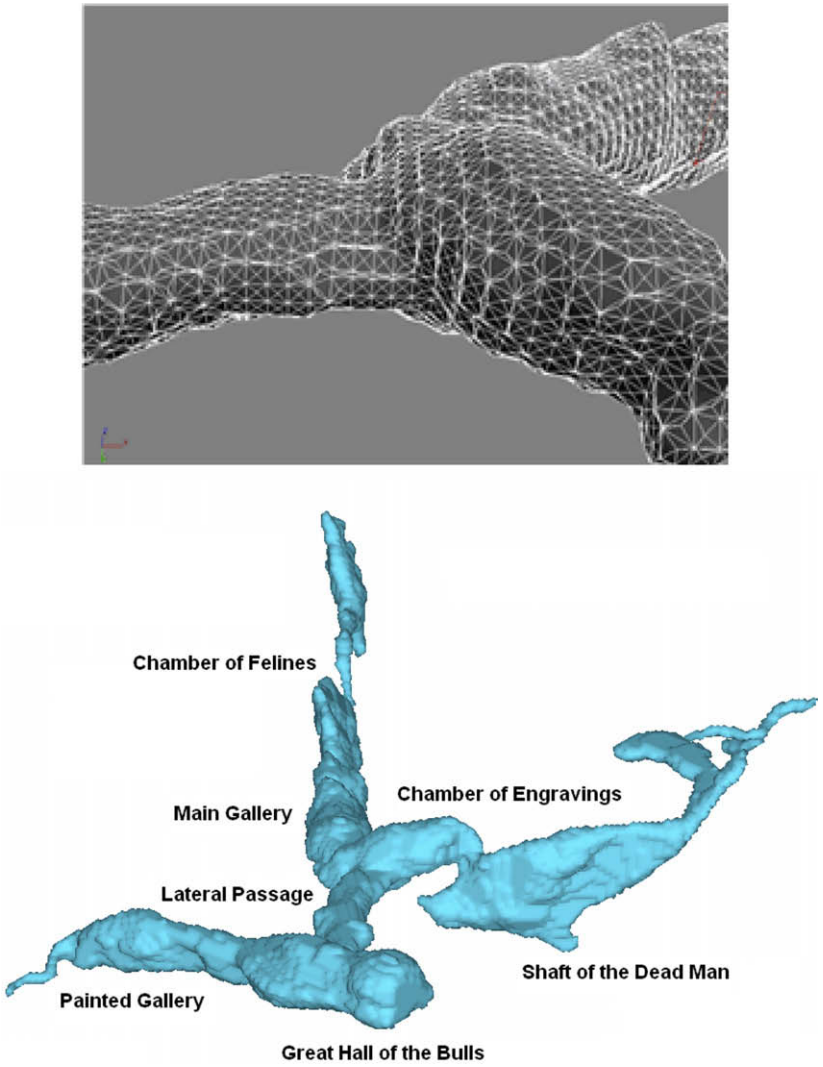

Fig. 11. Detail of the triangularized surface on the Lagrangian grid (top), topology of the Lascaux cave as considered in the simulation – several reference marks (bottom).

Table 1
Comparison between theoretical V_0 and simulated V values of velocities in the boundary layer of a differentially heated square cavity.

Ra	10^2	10^3	10^4	10^5	10^6	10^7	10^8
V_0 (m/s)	1.8610^{-2}	2.7410^{-2}	4.0210^{-2}	5.910^{-2}	8.610^{-2}	1.2710^{-1}	1.8710^{-1}
V (m/s)	8.710^{-4}	3.810^{-3}	9.410^{-3}	1.510^{-2}	2.210^{-2}	3.310^{-2}	4.910^{-2}

Table 2
Comparison between reference Nu_{ref} and our simulated values Nu of Nusselt numbers in the boundary layer of a differentially heated square cavity.

Ra	10^2	10^3	10^4	10^5	10^6	10^7	10^8
Nu_{ref} [30]				4.521	8.8252	16.523	30.225
Nu	1.0015	1.1178	2.2448	4.5217	8.8252	16.523	30.225

years above the cave, and those taken in the cave since 1963. A computerized system using a remote metering has been set up in the cave to record the variations in temperature, hygrometry and carbon dioxide gas pressure.

Two climatic configurations are chosen, corresponding to two different periods, September 1981, during which the cavity remains in a stable state, and December 1999, before the work of replacement of the air treatment machine [33]. Profiles of temperature are given in Fig. 12 as a function of depth. These two periods are representative of two very different configurations. September 1981 represents the typical behavior of the 1980s, while December 1999 corresponds to the 1990s and early 2000s, whatever is the season in the year.

Fig. 13 shows the different distribution of temperature depending on the climatic configuration along the Y direction.

In September 1981, the slope of temperature is positive, inside the cave the vaults are colder than the cave floor. In December 1999, the slope is negative, the cave floor being colder than the vaults.

Once the temperature gradient is introduced in the calculation domain (including the cave and the surrounding rock) the flow induced by natural convection is established in the cavity.

4.1.3. Physical characteristics

The humidity is initialized to a value of 98% of relative moisture content in the whole cave. The calculations are made on the absolute moisture content, related to the temperature at each point. The diffusion coefficient of the moisture in air is $D = 2.18\times 10^{-5}$ m/s.

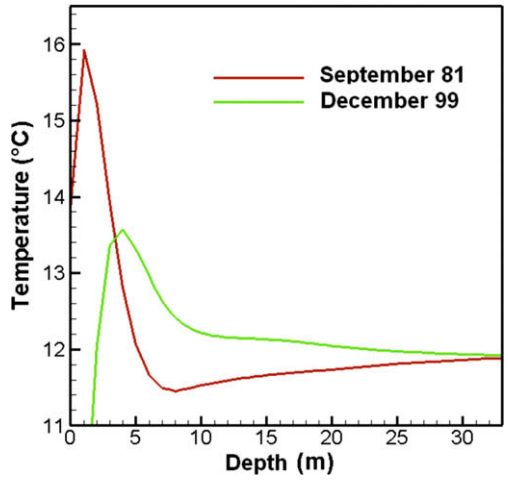

Fig. 12. Temperatures following a one-dimensional heat conduction model in the rock as a function of depth.

The characteristics of the rock and air are the following: $\rho_s = 1800$ kg/m^3, $C_{Ps} = 1000$ J/kg K, $\lambda_s = 1$ W/m K, $\rho_a = 1.1768$ kg/m^3, $\mu_a = 1.85\times 10^{-5}$ Pa s, $C_{Pa} = 1006$ J/kg K, $\lambda_a = 0.0263$ W/m K.

4.2. Results and analysis

The simulation is dedicated here to measure the impact of the local outside climate change on the management of the climate in the cave. Between 1965 and 1981, the temperature gradient in the cave met the requirements of the operational plan as set out by the Scientific Commission. In winter, the air temperature increases from the surface to the lower areas of the cave, whereas in summer this order is maintained artificially by deliberately lowering the air in the Machine Room, located before the Great Hall of the Bulls. Since 1981, temperature distribution changed, temperatures in the lower parts of the cave became lower than the mean surface temperatures (the thermal inertia of the ground increases as its thickness increases). The natural temperature gradient is inverted. This phenomenon is independent of the artificial control system of the cave and is related only to the outside weather pattern.

The temperature distribution in the cave is homogeneous in the thermal configuration of September 1981, as it can be seen in Fig. 14, where are exhibited zones of convective currents. The mean velocity values are approximately 10^{-2} m/s. Whereas in December 1999, in Fig. 14, the temperature is stratified, and no major convection current is noticed, due to the inversion of the temperature gradient between the two dates (Fig. 13). In this case, velocities are 100 times lower, around 10^{-4} m/s.

One of the major problem concerning the conservation of the Lascaux cave is its evolving state. A porous rock in equilibrium with a humid atmosphere is classically more or less saturated with water. Under certain conditions, the water vapor contained in the air present in the network of rock pores can condense. This liquid water is fixed by capillary action in the smallest pores, the pores for which the radius is less than a function of the relative moisture of the air. The condensed water contained in the pores is aggressive and a chemical equilibrium is reached by dissolution of carbonate minerals in the rock. Once saturated, this water remains inert as long as the atmospheric pressure, the temperature and the partial pressure of carbon dioxide is unchanged. When this equilibrium is broken, a drop would evaporate and this process would then result in precipitation of calcite. The condensation–evaporation cycle can occur repeatedly and lead to a loss of carbonates from the porous matrix, causing a major issue of conservation. These observations have demonstrated the need to avoid creating conditions in which rock dissolution and calcite deposition are promoted and to strive to maintain the most stable possible air conditions, while taking into account the natural rhythms of the cave.

The aim of the simulation is to give information about the precise location of the condensation risk zones. The case presented here corresponds to the configuration without anthropogenic effects. It is meant to serve as a basis for further studies, as the introduction of a machinery, human presence, and hot and cold points.

The moisture content distribution on the walls of the cave for the two climatic conditions described before is given in Fig. 16. Its distribution in a view of the right gallery, from the lateral Passage towards the Chamber of Felines for the two previous climatic

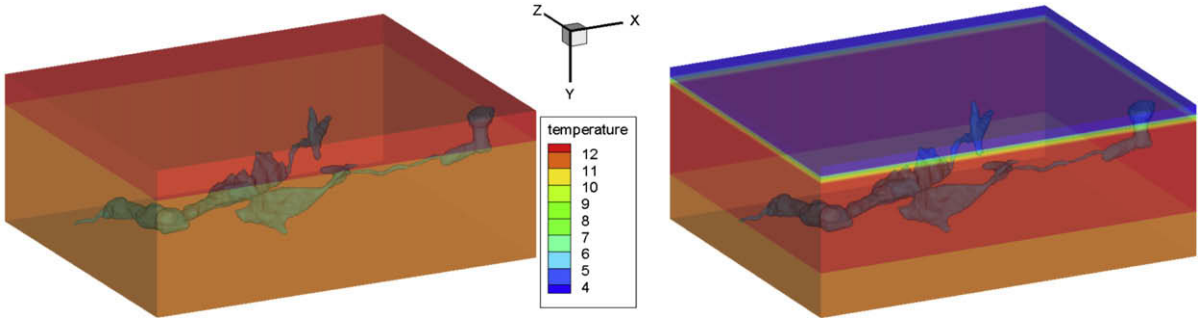

Fig. 13. Visualization of the temperature profiles for both climatic configurations, September 1981 (a) and December 1999 (b).

configurations is given in Fig. 17. In the case of September 1981 (Figs. 16 and 17) the absolute moisture content is higher in the vaults than on the floor, whereas in December 1999 (Figs. 16 and 17) the moisture is concentrated in the floor. This accurate description allows to know the places where the condensation risk is higher, before any introduction of external disturbance. The slice concerning the right gallery shows the spatial evolution of the absolute moisture content depending on the thermal configuration. In 1981, there are homogeneous zones, while in 1999, we found layers of different absolute moisture contents, due to the inversion of temperature.

Moreover, the climatic configuration of December 1999 corresponds to a higher global absolute moisture content than the one of September 1981.

The distribution of temperature and their values directly influence the moisture content field. In September 1981, the vaults are colder than the floor, inducing a concentration of moisture in the vaults with a higher value. In December 1999, the distribution of temperature is reversed, thus the distribution of moisture is also reversed, following the value of temperature. Nevertheless, inside the cave, concentration lines do not follow iso-temperatures, as it can be observed in Fig. 18. The moisture content is transported by the air.

Furthermore, the inversion of temperature implies a drastic modification of natural convection, and of the intensity of the velocities. Indeed, in September 1981, the air flows from the floor to the vaults increase the moisture concentration in this zone, whereas in December 1999 the very low velocities lead to a stagnation of the layers of moisture, on the floor of the cave.

The convective currents are closer studied in Fig. 15. A slice taken from the right part of the cave, in the Main Gallery, presents the normalized velocity and several streamlines. The velocity is higher on the walls, and distinct convective currents can be observed. A different view of the situation is also presented in this figure, virtual particles are released in the right part of the cave, and their trajectory is related to the temperature by the color of the ribbon. The natural convection occurs both from the ground to the vaults and from the Great Hall of the Bulls to the end of the Main Gallery. The resulting currents are complex and fully three-dimensional, with a general convection from the lateral Chamber of Felines towards the Lateral Passage, and several smaller ones, isolated and corresponding to a convection going from the ground to the vaults.

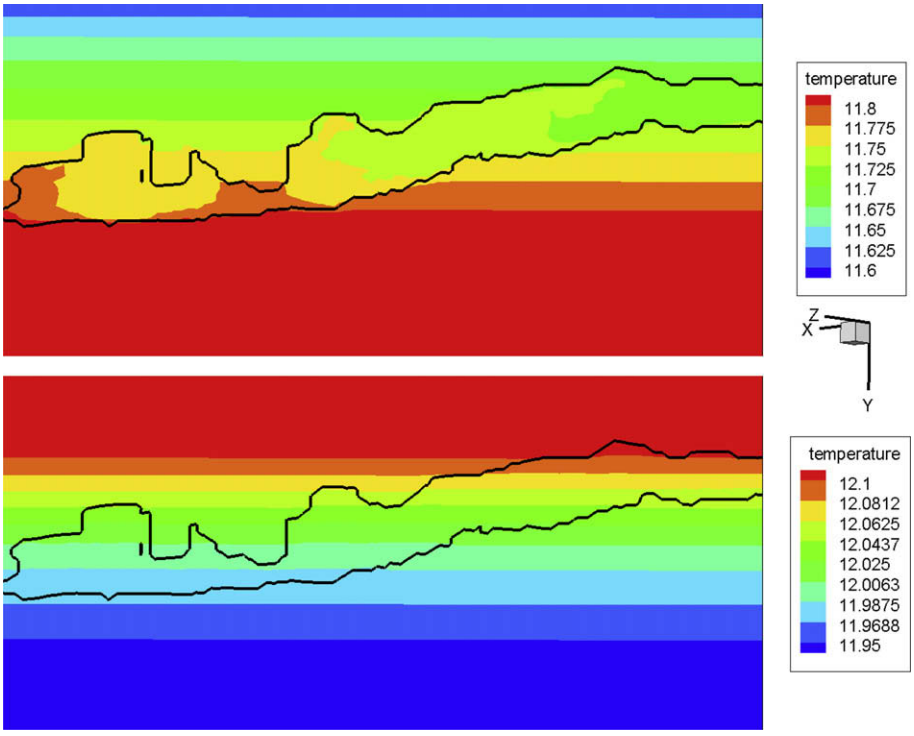

Fig. 14. Temperature distribution on a view of the right gallery, from the lateral Passage towards the Chamber of Felines for the climatic configuration of September 1981 in which $V \approx 10^{-2}$ m/s (top) and December 1999 in which $V \approx 10^{-4}$ m/s (bottom).

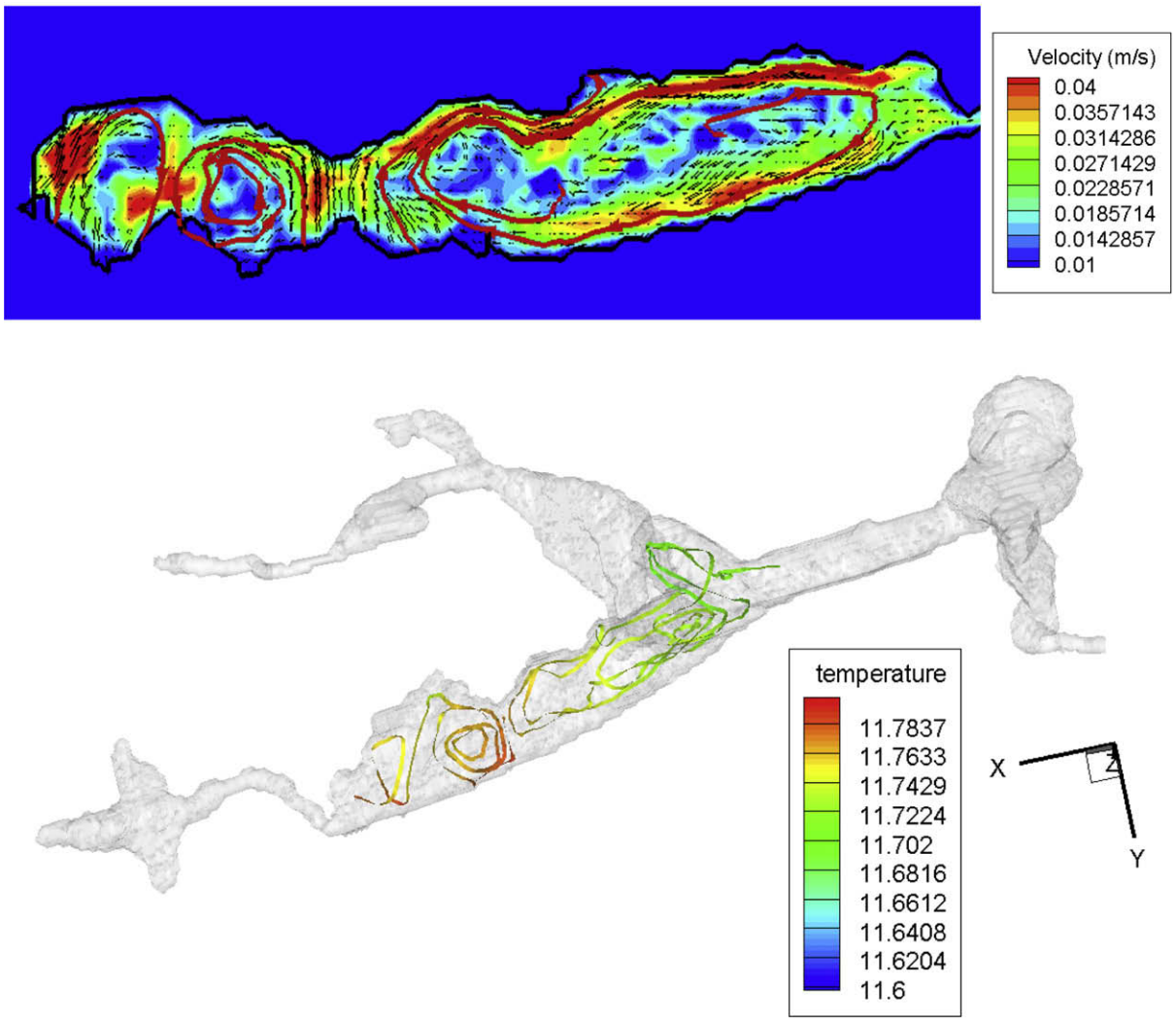

Fig. 15. Velocity distribution on the right gallery of Lascaux cave for the climatic configuration of September 1981, on a slice with the convective currents in red (top) and on a general view with the trajectory of a virtual particle on a ribbon colored with the temperature of the air crossed (bottom).

Finally, these numerical results have been validated by observations in the cave at the two climatic periods. In 1981, no major problem was noticed, whereas in the late 1990s and early 2000s, a spread of micro-organisms caused conservation issues. It can be assumed that the consequences of the increase and reverse of temperatures, i.e. drastic decrease of velocities and increase of

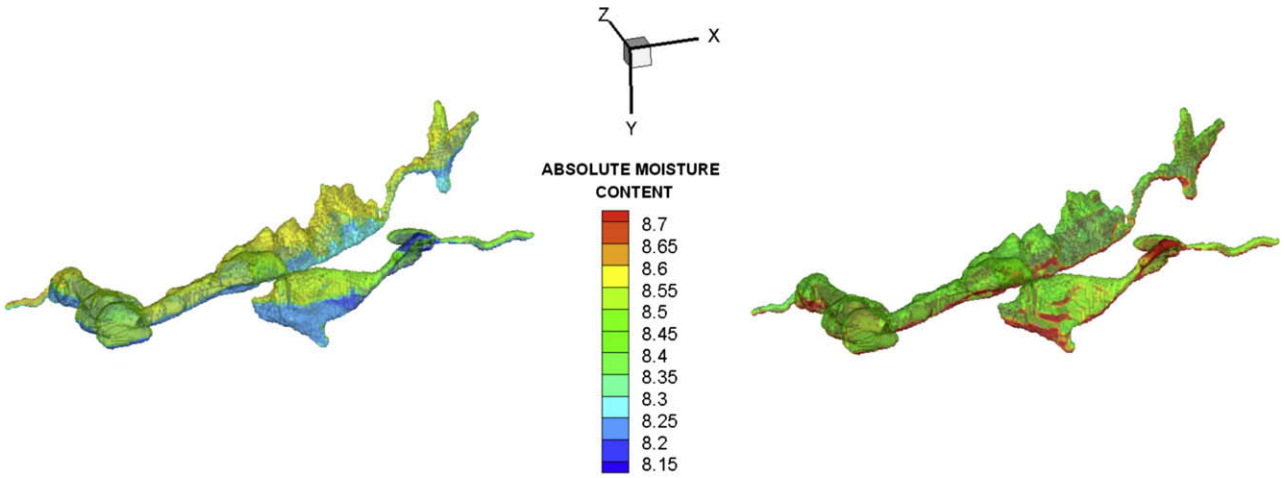

Fig. 16. Absolute moisture content on the walls of the cave for the climatic configuration of September 1981 (top) and December 1999 (bottom).

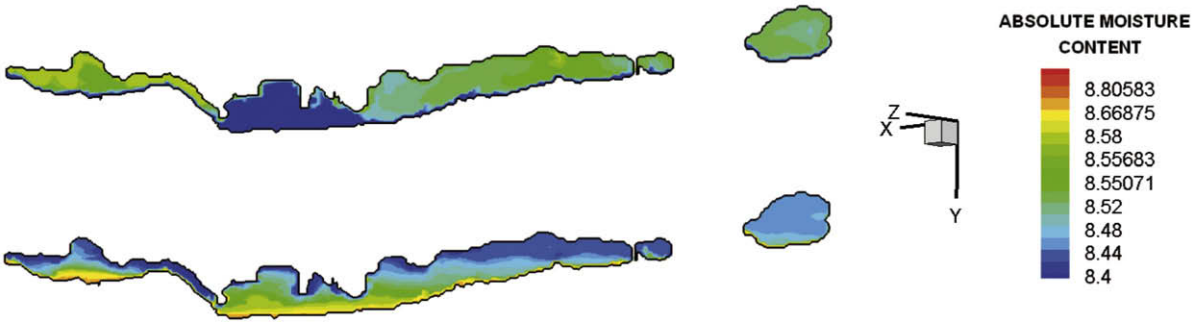

Fig. 17. Absolute moisture content on a view of the right gallery, from the lateral Passage towards the Chamber of Felines for the climatic configuration of September 1981 (top) and December 1999 (bottom).

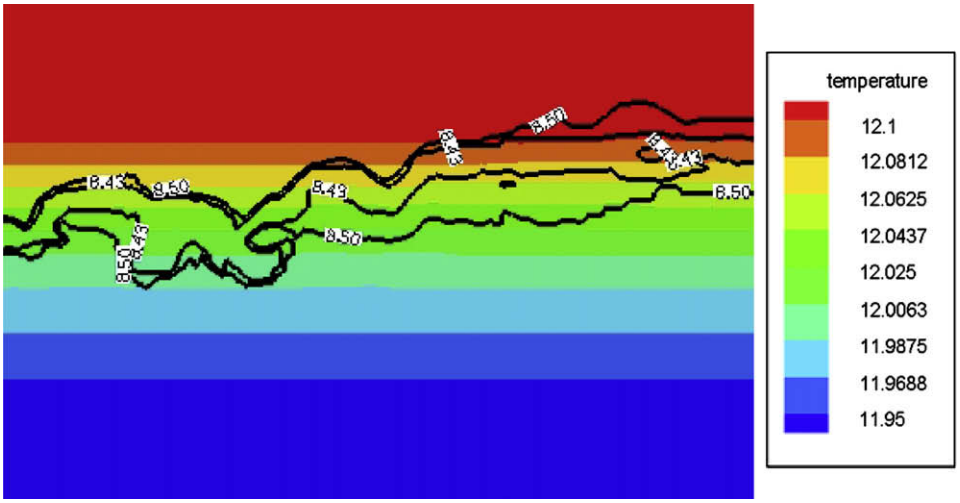

Fig. 18. Superposition of temperature and concentration distribution on a view of the right gallery, from the lateral Passage towards the Chamber of Felines for the climatic configuration of December 1999.

absolute moisture content, implied a stagnation of the air among the cavity and favored the development of micro-organisms.

5. Conclusions

An Eulerian/Lagrangian method for the numerical simulation of incompressible convection flows interacting with complex obstacles has been successfully validated on several natural convection cases, then applied here to the conservation of the Lascaux cave.

It has been shown in this article that a fictitious domain approach method coupled to a Lagrangian grid of obstacles allowed the correct description of the interaction between the natural convection flows and these obstacles. For example, a cavity filled with a large amount of cylinders shows the thermal comportment of a porous medium. Compared to experiments of natural convection (Sierpinski carpet) interacting with obstacles set according to fractal patterns, experimental measurements are found in good agreement with the penalization method with a precision lower than 20%. It can be due to the fact that the numerical boundary limits are slightly different than the experimental ones. Moreover, it has been pointed out that the two dimension hypothesis was not entirely valid and that three dimension simulations brought better results.

Concerning the application to the Lascaux cave, the article provided the first simulations of the entire geometry of the cavity, with a fictitious domain approach method. The results are confirmed by the observations made in the cave: it is more confined in the present thermal configuration than in the 1980s. The climate change made the cave more sensitive to disturbances. For example, the influence of humans entering the cave will be more devastating for the paintings in the present configuration than before.

Numerical perspectives are numerous. Higher order penalization will be implemented, by a technology currently under development, in order to better take into account the complex geometry of the objects at a scale lower than the grid. Our purpose is also to integrate moving obstacles in our simulations in order to take into account the impact of the moving of a human visiting the cave for example.

Acknowledgements

Electricité de France (EDF) within the framework of the scientific and technological sponsorship policy has provided the Ministry for the Arts the competence and the means of its own teams in partnership with the University of Bordeaux 1 and the Centre National de la Recherche Scientifique (CNRS) to understand and foresee the thermal and aeraulic effects inside the Lascaux cave. The authors also wish to thank the IDRIS and CINES (No. TER2237-2006) for their computer support.

References

[1] P. Chow, M. Cross, K. Pericleous, A natural extension of the conventional finite volume method into polygonal unstructured meshes for CFD application, Appl. Math. Model. 20 (2) (1996) 179–183.

[2] S.R. Mathur, J.Y. Murthy, A pressure-based method for unstructured meshes, Numer. Heat Transfer 31 (2) (1997) 195–215.
[3] K. Khadra, P. Angot, S. Parneix, J.P. Caltagirone, Fictitious domain approach for numerical modelling of Navier–Stokes equations, Int. J. Numer. Methods Fluids 34 (2000) 651–684.
[4] T.N. Randrianarivelo, G. Pianet, S. Vincent, J.P. Caltagirone, Numerical modelling of solid particle motion using a new penalty method, Int. J. Numer. Methods Fluids 47 (2005) 1245–1251.
[5] C. Peskin, The immersed boundary method, Acta Numer. 11 (2000) 479–517.
[6] R. Glowinski, T.W. Pan, T.I. Hesla, D.D. Joseph, A distributed Lagrange multiplier/fictitious domain method for particulate flows, Int. J. Multiphase Flows 25 (1999) 755–794.
[7] X. Zhong, A new high-order immersed interface method for solving elliptic equations with imbedded interface of discontinuity, J. Comput. Phys. 255 (2007) 1066–1099.
[8] A. Sarthou, S. Vincent, J.P. Caltagirone, P. Angot, Eulerian/Lagrangian grid coupling and penalty methods for the simulation of multiphase flows interacting with complex objects, Int. J. Numer. Methods Fluids 56 (8) (2008) 1093–1099.
[9] I. Ramiere, P. Angot, M. Belliard, A general fictitious domain method with immersed jumps and multilevel nested structured meshes, J. Comput. Phys. 225 (2007) 1347–1387.
[10] J. Brunet, P. Malaurent, J. Vouvé, Lascaux, histoire d'un difficile sauvetage, Archéologia 332 (1997) 24–35.
[11] M.A. Sire, Des restaurateurs au chevet des peintures de Lascaux, De l'élimination des champignons au constat d'tat, Les grottes ornées Monumental 2006 Monum Editions du Patrimoine 2 (2006) 68–75.
[12] G. Orial, J.D. Mertz, Lascaux: une grotte vivante, Étude et suivi des phénomènes microbiologiques, Les grottes ornées Monumental 2006 Monum Editions du Patrimoine 2 (2006) 76–78.
[13] P. Malaurent, R. Lastennet, J. Brunet, Une grotte sous influence: l'environnement hydrogéologique et climatique de la grotte de Lascaux Les grottes ornées Monumental 2006 Monum Editions du Patrimoine 2 (2006) 88–93.
[14] C. Ferchal, Modélisation des écoulements et des transferts de masse et de chaleur dans la grotte de Lascaux, Ph.D. Thesis, University of Bordeaux, Talence, France, 2003.
[15] C. Ferchal, J.-B. Ritz, J.P. Caltagirone, Ph. Malaurent, Simulation des écoulements et transferts de masse et de chaleur dans la Grotte de Lascaux, Congrès de la Société Francaise de Thermique, Grenoble, 3–6 juin, 2003.
[16] D. Lacanette, P. Malaurent, J.P. Caltagirone, S. Vincent, A model of thermal and aeraulic flows in the cave of Lascaux, International Association for Mathematical Geology XIth International Congress Université de Liège – Belgium, 2006.
[17] D. Lacanette, J.P. Caltagirone, Le simulateur Lascaux: un outil d'aide à la décision pour l'avenir de la préhistoire, Les grottes ornées Monumental 2006 Monum Editions du Patrimoine 2 (2006) 94–97.
[18] E. Arquis, J.-P. Caltagirone, On hydrodynamic conditions near a fluid-porous interface: application to the natural convection, Comptes Rendus de l'Académie des Sciences Série II b Mécanique 299 (1984) 1–4.
[19] S. Shin, D. Juric, Modeling three-dimensional multiphase flow using a level-contour reconstruction method for front tracking without connectivity, J. Comput. Phys. 180 (2002) 427–470.
[20] S.V. Patankar, Numerical Heat Transfer and Fluid Flow, Hemisphere Publishing Corporation, New York, USA, 1980.
[21] F.H. Harlow, J.E. Welsh, Numerical calculation of time-dependent viscous incompressible flow with free surface, Phys. Fluids 8 (1965) 2182–2189.
[22] M. Fortin, R. Glowinski, Méthodes de lagrangien augmenté, Application à la résolution numérique de problèmes aux limites, Dunod, 1982.
[23] I. Gustafsson, On first and second order symmetric factorization methods for the solution of elliptic difference equations, Technical Report, Chalmers University of Technology, 1978.
[24] H.A. Van Der Vorst, Bi-cgstab: a fast and smoothly converging variant of bi-cg for the solution of non-symmetric linear systems, SIAM J. Sci. Stat. Comput. 13 (1992) 631–644.
[25] S. Vincent, J.P. Caltagirone, P. Lubin, T.N. Randrianarivelo, An adaptative augmented Lagrangian method for three-dimensional multimaterial flows, Comput. Fluids 33 (2004) 1273–1289.
[26] S. Vincent, T.N. Randrianarivelo, G. Pianet, J.P. Caltagirone, Local penalty methods for flows interacting with moving solids at high Reynolds numbers, Comput. Fluids 36 (2007) 902–913.
[27] S. Vincent, J.P. Caltagirone, A one cell local multigrid method for solving unsteady incompressible multi-phase flows, J. Comput. Phys. 163 (2000) 172–215.
[28] E. Arquis, Transferts en milieu poreux et à l'interface: de l'échelle microscopique à l'échelle macroscopique, Ph.D. Thesis, University of Bordeaux, Talence, France, 1994.
[29] A. Amine, J.K. Platten, M. Hasnaoui, Thermal convection around obstacles: the case of Sierpinski carpets, Exp. Fluids 36 (2004) 717–727.
[30] P. Le Quéré, Accurate solutions to the square thermally driven cavity at high Rayleigh numbers, Comput. Fluids 20 (1991) 29–41.
[31] J. Taine, J.P. Petit, Transferts thermiques: Mécanique des fluides anisothermes, Dunod, 1989.
[32] Website: www.meteo.fr.
[33] P. Malaurent, J. Brunet, D. Lacanette, J.P. Caltagirone, Contribution of numerical modelling of environmental parameters to the conservation of prehistoric cave paintings: the example of Lascaux Cave, Conserv. Manage. Archaeol. Sites 8 (2006) 1–11.